Caging ruthenium complexes with non-toxic ligands for photoactivated chemotherapy
Cuello Garibo, J.A.

Citation
Cuello Garibo, J. A. (2017, December 19). *Caging ruthenium complexes with non-toxic ligands for photoactivated chemotherapy*. Retrieved from https://hdl.handle.net/1887/58688

Cover Page

The handle http://hdl.handle.net/1887/58688 holds various files of this Leiden University dissertation.

Author: Cuello Garibo J.A
Title: Caging ruthenium complexes with non-toxic ligands for photoactivated chemotherapy
Issue Date: 2017-12-19

6

PACT or PDT: are ruthenium(II) complexes photosubstituting a non-toxic ligand also phototoxic under hypoxic conditions?

The cytotoxicity of a series of ruthenium complexes with a photolabile non-toxic N,S ligand is tested in human cancer cells under hypoxia (1% O_2) to investigate the oxygen-dependency of their activity. All compounds show lower cytotoxicity under hypoxia (1% O_2) compared to that under normoxia (21% O_2), probably due to the chemoresistance acquired by cancer cells at 1% O_2. The cytotoxicity of some PACT compounds was clearly enhanced after green light irradiation, which is the first experimental demonstration of light-induced cytotoxicity under hypoxia for a metal-based PACT compound releasing a non-toxic organic ligand.

6.1 Introduction

Ruthenium-based Photoactivated Chemotherapy (PACT) is a new, oxygen-independent phototherapy modality against cancer that relies on the breakage of a bond to generate a species that is more cytotoxic than the prodrug. Many examples of PACT agents have been reported in literature and the observed *in vitro* cytotoxicity is usually attributed, by analogy with cisplatin, to the photogenerated aqua complex after photosubstitution of a bidentate ligand.[1-3] However, two major questions are often not addressed in the literature. First, what is the actual cytotoxic species after a photoreaction that has generated two photoproducts: the aquated metal complex or the released organic ligand?[4] Secondly, can the observed cytotoxic effect be ascribed to the generation of even small amounts of singlet oxygen ($^1O_2$)? In Chapter 3 and Chapter 4, we have addressed the first question using new ruthenium polypyridyl complexes bearing non-cytotoxic N,S ligands that, upon light irradiation, are substituted by two water molecules. Furthermore, quantum yields for $^1O_2$ generation (Φ_Δ) have systematically been measured for all ruthenium(II) complexes, usually leading to Φ_Δ values lower than 0.05, while ruthenium complexes used as PDT agents have Φ_Δ values typically above 0.50.[5-6] In this chapter, we address the second question, and try to understand whether Φ_Δ values as low as 0.05 can play a role in the observed phototoxicity of "PACT-like" ruthenium compounds.

Due to the oxygen-independent character of PACT, a true PACT-agent should work also in absence of oxygen in the irradiated tissues. On the contrary, in PDT the photocytotoxicty of a photosensitizer is usually impaired under hypoxia.[7] Hypoxia occurs in tumors due to the poorly vascularized nature of many primary tumors, coupled to the low diffusion of oxygen in non-vascularized tissues. However, biologically speaking hypoxia does not only point to the absence of dioxygen in the irradiated tissues. The lack of dioxygen has indeed a great impact on cancerous or non-cancerous cells, as it changes many aspects of their biology.[8] For example, the upregulation of hypoxia-inducible factors (HIFs) has consequences on the cell metabolism, invasion properties, cell death modes, or membrane integrity, among others.[9-11] Furthermore, tumour radiotherapy has a lower efficiency in hypoxic tissues, where the radiosensitizing properties of molecular oxygen are missing.[12] A recent report from Lameijer *et al.*[13] demonstrated for the first time that ruthenium-based PACT compounds remained as efficient under hypoxia (1% O_2) as under normoxia (21% O_2): the photo index (PI) of [Ru(tpy)(biq)(STF-31)]Cl_2 (tpy = 2,2';6',2"-terpyridine and biq = 2,2'-biquinoline), in which the ligand STF-31 is an organic

inhibitor of nicotinamide phosphoribosyl transferase (NAMPT), was comparable when irradiation was performed in hypoxic or normoxic conditions.[13] In this report, the photocytotoxicity was primarily due to NAMPT inhibition by the organic STF-31 ligand generated upon light irradiation. To our knowledge, there is no experimental report of PACT under hypoxia where the photocytotoxicity is due to the photogenerated metal-based fragment.

In this chapter, we investigate the oxygen dependency of the cytotoxicity of a series of structurally related ruthenium(II) PACT complexes of which the ligand that is photosubstituted, 2-(methylthio)methylpyridine (mtmp), is non-toxic. The series of complexes, shown in Figure 6.1 comprises $[Ru(Ph_2phen)_2(mtmp)]Cl_2$ (Ph_2phen = 4,7-diphenyl-1,10-phenanthroline, $[\mathbf{1}]Cl_2$), $[Ru(bpy)(Ph_2phen)(mtmp)](PF_6)_2$ (bpy = 2,2'-bipyridine, $[\mathbf{2}](PF_6)_2$), $[Ru(dmbpy)_2(mtmp)]Cl_2$ (dmbpy = 6,6'-dimethyl-2,2'-bipyridine, $[\mathbf{3}]Cl_2$), and $[Ru(bpy)(phpy)(mtep)]PF_6$ ($phpy^-$ = 2-phenylpyridine, mtep = 2-(methylthio)ethyl-2-pyridine, $[\mathbf{4}]PF_6$). The synthesis and photochemistry of the new complexes $[\mathbf{2}](PF_6)_2$ and $[\mathbf{3}]Cl_2$ is described, while $[\mathbf{1}]Cl_2$ and $[\mathbf{4}]PF_6$ were already reported in Chapter 3 and Chapter 5, respectively. In Chapter 3 we showed that mtmp is non-toxic below 150 µM, and that irradiation of $[\mathbf{1}]^{2+}$ leads to the photosubstitution of mtmp by two water molecules. Such photoreactivity translated in lung cancer cells (A549 cell line) into a low effective concentration (EC_{50}), i.e. the compound concentration (in µM) that reduces cell viability by 50% compared to untreated cells, of 0.48 µM upon light irradiation but a photo index (PI) of only 6, which was attributed to the high lipophilicity of the complex, leading to high uptake and high dark toxicity. The tris-heteroleptic complex $[\mathbf{2}]^{2+}$ is designed to solve this issue: with only one Ph_2phen ligand the lipophilicity and dark cytotoxicity of this complex is expected to decrease, while the photosubstitution typical for PACT should be retained. On the other hand, in Chapter 4 we demonstrated that $[Ru(dmbpy)_2(mtpa)]^{2+}$ (mtpa = 3-(methylthio)propylamine) had an EC_{50} value of 44 µM against A549 cells after light irradiation, and that the complex was lipophilic enough to cross the cell membrane. However, it was not thermally stable, so that similar EC_{50} values were obtained in the dark. By replacing the primary amine by a pyridine in the N,S ligand, we designed $[\mathbf{3}]^{2+}$ so that it may have an enhanced thermal stability and thus a higher PI. All complexes $[\mathbf{1}]^{2+} - [\mathbf{4}]^{2+}$ should thus show similar photosubstitution behaviour; their cytotoxicity was tested against A549 cells and prostate cancer cells (PC3pro4 cell line) under hypoxia, and compared to normoxic conditions. The activity of these PACT compounds was compared to that of Rose Bengal, a commercially available PDT type II photosensitizer, and to that of the ruthenium-based photosensitizer

[Ru(Ph$_2$phen)$_2$(bpy)]Cl$_2$ ([**5**]Cl$_2$), a structurally similar photosensitizer incapable of ligand substitution. A structure-function relationship is discussed.
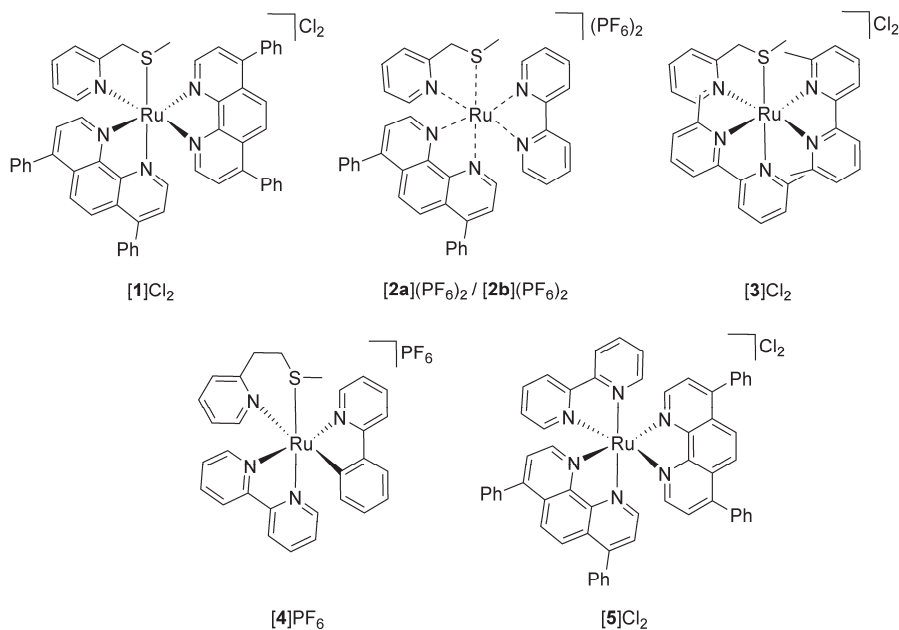

[**1**]Cl$_2$ [**2a**](PF$_6$)$_2$ / [**2b**](PF$_6$)$_2$ [**3**]Cl$_2$

[**4**]PF$_6$ [**5**]Cl$_2$

Figure 6.1. Schematic structures of the complexes [1]Cl$_2$, [2](PF$_6$)$_2$, [3]Cl$_2$, [4]PF$_6$, and [5]Cl$_2$ described in this Chapter. For complex [2](PF$_6$)$_2$ the configuration is not specified, and the notation [2]$^{2+}$ represents two undefined isomers [2a]$^{2+}$ and [2b]$^{2+}$, where the sulfur atom can be either trans to bpy or to Ph$_2$phen (see Appendix VII). For clarity, only the Λ enantiomer of the complexes is represented, but all compounds were synthesized and used as racemates.

6.2 Results

6.2.1 Synthesis

The synthesis of complexes [**1**]Cl$_2$, [**4**]PF$_6$, and [**5**]Cl$_2$ was performed as described in Chapter 3, Chapter 5, and in literature.[14] The synthesis of [**2**](PF$_6$)$_2$ was adapted from a method developed by Keyes *et al.* for the synthesis of tris-heteroleptic bidentetate ruthenium complexes [Ru(L$_1$)(L$_2$)(L$_3$)]$^{n+}$.[15] The novelty of this method, in which the three different bidentate ligands L$_1$, L$_2$, and L$_3$ are coordinated sequentially, relies on the coordination of an oxalate ligand (ox^{2-}) during the coordination of the second bidentate ligand L$_2$ in order to prevent the formation of [Ru(L$_1$)(L$_2$)$_2$]$^{n+}$, in which two identical ligands L$_2$ coordinate to the metal. Here, the order of addition of the ligands was first Ph$_2$phen, then mtmp, and finally bpy. Details of the synthesis can be found in Appendix VII. After the addition of bpy, due to the dissymetry of mtmp and the tris-heteroleptic nature of the complex, two configurational isomers are expected: one

having the sulfur donor atom *trans* to bpy and another having the sulfur donor atom *trans* to Ph$_2$phen. Thus, two isomers were obtained according to ^{1}H NMR and were separated by column chromatography: isomer [**2a**](PF$_6$)$_2$, which was contaminated with [Ru(Ph$_2$phen)(bpy)$_2$](PF$_6$)$_2$, and isomer [**2b**](PF$_6$)$_2$, which was NMR pure but obtained in a low yield (<2%). As shown in Figure AVII.1 and explained in Appendix II, the exact configuration of the two isomers could not be established. In photochemical and biological experiments, a mixture of both isomers [**2b**]$^{2+}$:[**2a**]$^{2+}$ in a ratio 1:0.23, further indicated as [**2**](PF$_6$)$_2$, was used.

Compound [**3**]Cl$_2$ was obtained by reacting [Ru(dmbpy)$_2$Cl$_2$] with mtmp in ethylene glycol at 100 °C for 15 min. The complex was isolated by precipitation of the hexafluoridophosphate salt ([**3**](PF$_6$)$_2$), and then reconverted into the chloride salt by precipitation of [**3**]Cl$_2$ in acetone after addition of Bu$_4$NCl. Single crystals suitable for X-ray structure determination were obtained for [**3**]Cl$_2$ by slow vapour diffusion of diisopropyl ether into a solution of the compound in methanol. The structure crystallizes in the centrosymmetric space group P-1 and the crystal lattice contains both enantiomeric configurations Λ-(*S*) and Δ-(*R*) of the complex [Ru(dmbpy)$_2$(mtmp-κN,κS)]Cl$_2$·CH$_3$OH·H$_2$O. The molecular structure, shown in Figure 6.2, shows that the configuration adopted by the chiral sulfur atom lowers the steric clash between the methyl group of the thioether and that of the dmbpy ligand. Furthermore, the structure shows a longer Ru-S bond (2.3709(4) Å, see Table AVII.1) and Ru-N bonds (between 2.0928(12) and 2.1362(12) Å), than those observed in the crystal structure of the non-strained analogue [Ru(3,3'-dmbpy)$_2$(mtmp)]$^{2+}$ (3,3'-dmbpy = 3,3'-dimethyl-2,2'-bipyridine) reported by Wallenstein *et al.* (Ru-S = 2.3262(9) Å and Ru-N between 2.062(2) and 2.095(2) Å).[16]
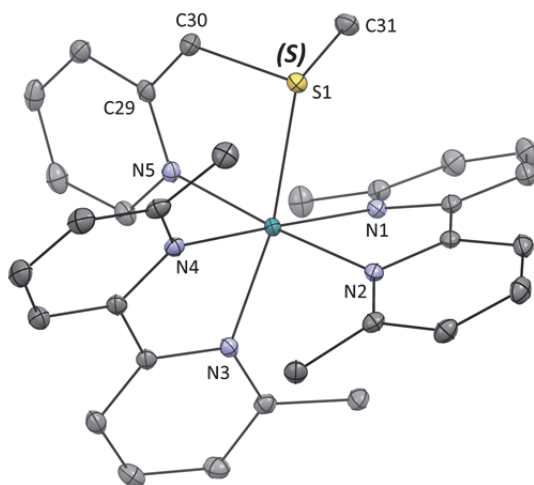
Figure 6.2. Displacement ellipsoid plot (50% probability level) of the Λ enantiomer of the cationic complex in the crystal structure of the pair Λ-(S)/Δ-(R)-[Ru(dmbpy)$_2$(mtmp-κN,κS)]Cl$_2$·CH$_3$OH·H$_2$O. The hydrogen atoms, chloride counteranions, lattice methanol and water molecules have been omitted for clarity. Selected bond distances and angles are reported in Table AVII.1.

6.2.2 Photoactivation and singlet oxygen generation

The photoreactivity of complexes [**1**]Cl$_2$ and [**4**]PF$_6$ has been described in Chapter 3 and Chapter 5, respectively. [**1**]Cl$_2$ shows photosubstitution of mtmp by two solvent molecules in water with a quantum yield of 0.0030. [**4**]PF$_6$ is only soluble in CH$_3$CN in which it shows selective photosubstitution of mtep by two CH$_3$CN molecules with a quantum yield of 0.00035. The photoreactivity of [**2**](PF$_6$)$_2$ was studied in CH$_3$CN due to its low solubility in water, and monitored with UV-vis spectroscopy. The spectrum of a solution of [**2**](PF$_6$)$_2$ irradiated for 20 min with green light (521 nm) showed an increase of the intensity of the MLCT band between 400 − 430 nm, and a decrease in the valley at 344 nm with isosbestic points at 363 nm and 440 nm (Figure 6.3a). After 15 min, when the reaction reached the steady state, mass spectrometry showed peaks at m/z = 140.3 and 336.3, corresponding to the free ligand {mtmp + H}$^+$ (calcd m/z = 140.1) and [Ru(bpy)(Ph$_2$hen)(CH$_3$CN)$_2$]$^{2+}$ (calcd m/z = 336.1), respectively. Thus, upon light irradiation in CH$_3$CN, mtmp is substituted selectively with a quantum yield of 0.111 (see Appendix I and Figure AVII.3).
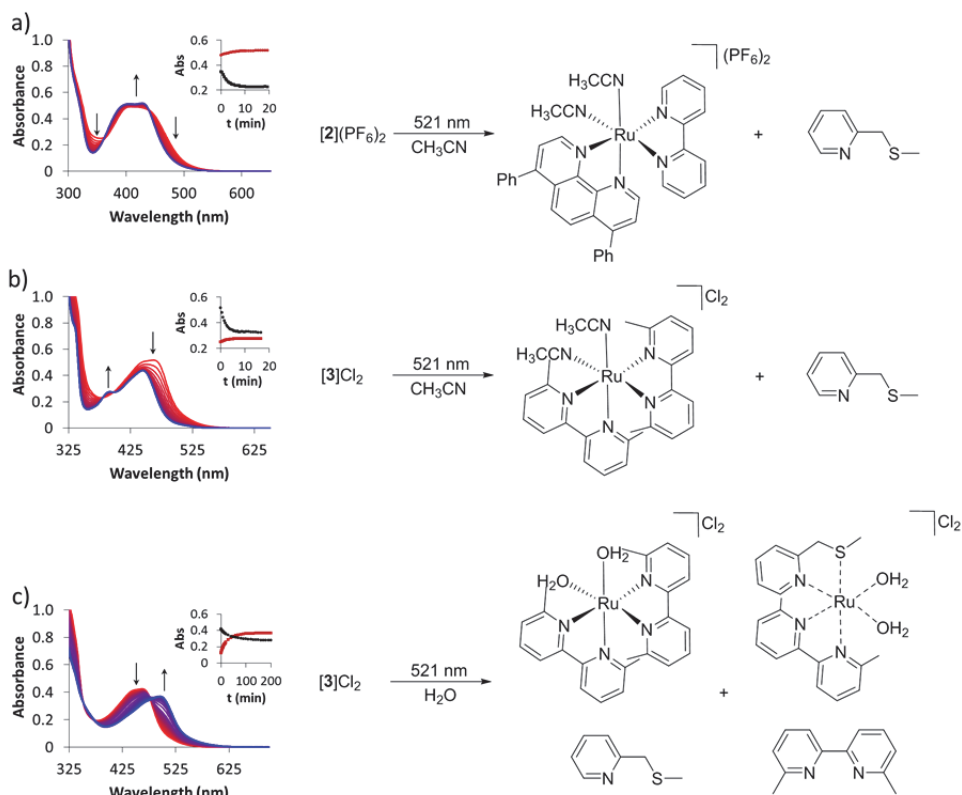
Figure 6.3. Evolution of the UV-vis spectra of solutions of a) [2](PF₆)₂ in CH₃CN (0.036 mM), b) [3]Cl₂ in CH₃CN (0.088 mM), and c) [3]Cl₂ in water (0.073 mM) upon irradiation with a 521 nm green LED (photon fluxes were $6.21 \cdot 10^{-8}$, $6.25 \cdot 10^{-8}$, and $2.39 \cdot 10^{-8}$ $mol \cdot s^{-1}$, respectively) under N_2. Inset: black dots represent the absorbance at 460 nm (a), 460 nm (b), and 450 nm (c) vs. time, and red squares represent the absorbance at 430 nm (a), 390 nm (b), and 500 nm (c) vs time.

For [3]Cl₂, irradiation with green light in CH₃CN resulted in a shift of the MLCT band of the UV-vis spectra from an absorption maxima of 462 nm to 444 nm and isosbestic points at 382 nm and 395 nm (Figure 6.3b). The steady state was reached after 10 min, and mass spectrometry at that point showed a single peak at m/z = 275.9 corresponding to $[Ru(dmbpy)_2(CH_3CN)_2]^{2+}$ (calcd m/z = 276.1). Thus, like in complex [2](PF₆)₂, upon light irradiation in CH₃CN mtmp is substituted selectively with a very high quantum yield of 0.348 (see Appendix I and Figure AVII.4). However, when the irradiation was performed in water, no clear isosbestic points were visible, which indicated the occurrence of either sequential or parallel photosubstitution reactions (Figure 6.3c). Indeed, mass spectrometry after 2.5 h irradiation showed peaks at m/z = 140.3, 185.5, 253.8, and 276.2 corresponding to $\{mtmp + H\}^+$ (calcd m/z = 140.1), $\{dmbpy + H\}^+$ (calcd m/z = 185.1), $[Ru(dmbpy)(mtmp)(CH_3CN)_2]^{2+}$ (calcd m/z =

125

253.6), and $[Ru(dmbpy)_2(CH_3CN)_2]^{2+}$ (calcd m/z = 276.1), respectively. The CH_3CN molecules come from the eluent used for the mass spectrometry as irradiation was performed in water. Thus, in water photosubstitution of mtmp and dmbpy occur in parallel, generating four photoproducts, *i.e.* mtmp, dmbpy, $[Ru(dmbpy)_2(OH_2)_2]^{2+}$ and $[Ru(dmbpy)(mtmp)(OH_2)_2]^{2+}$. Non-selective photosubstitution was already observed for $[Ru(bpy)(dmbpy)(mtpa)]^{2+}$ (Chapter 4), however, the dependence of selectivity on the solvent was not established yet.

In order to have a complete overview of the photoreactivity of these ruthenium complexes, the Φ_Δ was experimentally determined. $^1O_2$ is a highly reactive oxygen species (ROS) and it is the most common cytotoxic photoproduct in PDT type II.[17-19] Φ_Δ was determined under blue light irradiation (450 nm) by direct detection of the 1274 nm infrared phosphorescence of $^1O_2$ in CD_3OD using $[Ru(bpy)_3]Cl_2$ as reference ($\Phi_\Delta = 0.73$).[20] The Φ_Δ value for the PDT agent [**5**]Cl_2 is surprisingly high ($\Phi_\Delta = 0.95$,), whereas for the PACT complexes [**1**]Cl_2 and [**3**]Cl_2 low values of 0.020 and 0.027 were found, respectively (Table 6.1). For [**2**]$(PF_6)_2$ a significantly higher Φ_Δ value of 0.069 was found, which is unexpected due to the structural similarity with [**1**]Cl_2 or $[Ru(bpy)_2(mtmp)]Cl_2$ ($\Phi_\Delta = 0.023$, see Chapter 3). Finally, the cyclometalated compound [**4**]PF_6 showed a Φ_Δ value of 0.19, which is in accordance with its low photosubstitution quantum yield.

Table 6.1. Singlet oxygen generation quantum yields (Φ_Δ) of [1]Cl₂, [2](PF₆)₂, [3]Cl₂, [4]PF₆, [5]Cl₂, and Rose Bengal determined under blue light excitation (450 nm) by direct detection of the 1274 nm infrared phosphorescence of ¹O₂ in CD₃OD using [Ru(bpy)₃]Cl₂ as reference ($\Phi_\Delta = 0.73$).

	[1]Cl₂	[2](PF₆)₂	[3]Cl₂	[4]PF₆	[5]Cl₂	Rose Bengal
Φ_Δ	0.020	0.069	0.027	0.19	0.95	0.79[a]

[a]Value taken from Tanielian et al.[21]

6.2.3 Cytotoxicity assays and cell uptake

The cytotoxicity of the five complexes and Rose Bengal was first tested under normoxia against two different cancer cell lines (A549 and PC3pro4 cells) following a protocol reported by Hopkins *et al.*[22] and described in the Experimental Section. A549 is a human lung cancer cell line and PC3pro4 is a cancer cell line derived from a bone metastasis obtained after injection of PC3 human prostate cancer cells into nude mice.[23] For each compound the effective concentrations (EC_{50}), *i.e.* the compound concentration (in μM) that reduces cell viability by 50% compared to untreated cells, are listed in Table 6.3. Photo indeces (PI) were calculated as the ratio of EC_{50} obtained in the dark, divided by the values obtained after light irradiation.

Under normoxic conditions, Rose Bengal showed PI's higher than 40 and 400 for A549 and PC3pro4 cells, respectively, confirming its excellent photodynamic properties when there is no lack of dioxygen (21% O_2). For the photosensitizer [**5**]Cl_2, the higher cytotoxicity in the dark lowered the PI compared to Rose Bengal, with values of 13 and 29 for A549 and PC3pro4, respectively. On the other hand, for compounds [**1**]Cl_2, [**2**]$(PF_6)_2$, and [**3**]Cl_2 EC_{50} values in the dark of 3.4, 59, and >500 µM, respectively, were found for A549 cells. After green light irradiation, the EC_{50} values decreased to 0.62, 6.5, and 71 µM with PI's of 5.5, 9, and >7, respectively. Thus, the less lipophilic the complex is, the higher EC_{50} values were found both in the dark and after light activation. A similar trend was observed with PC3pro4 cells. For PACT compounds cytotoxicity is indeed closely related to cellular uptake and subcellular localization, which are in turn closely related to the lipophilicity of the prodrug.[24] Typically, the presence of more phenyl groups results in an increase of lipophilicity,[25] whereas the effect of methyl groups is less pronounced. Thus, [**2**]$(PF_6)_2$ showed similar uptake (Table 6.2) as [**1**]Cl_2, while cells were treated with solutions of very different concentration, *i.e.* 65 and 3.4 µM, respectively. Thus, due to the lower lipophilicity of [**2**]$(PF_6)_2$, a much higher concentration was necessary to obtain the same cellular uptake and biological activity as for [**1**]Cl_2. [**3**]Cl_2 was less efficiently taken up since a high concentration (160 µM) still resulted in a lower intracellular ruthenium concentration. This compound appeared to be the least toxic, both in the dark and after light activation.

Table 6.2. Cellular uptake of [1]Cl₂, [2](PF₆)₂, [3]Cl₂, [4]PF₆, and [5]Cl₂ in A549 cells upon treatment near the dark EC₅₀ value.

	[**1**]Cl_2	[**2**]$(PF_6)_2$	[**3**]Cl_2	[**4**]PF_6	[**5**]Cl_2
Treatment concentration (µM)	3.4	65	160	0.08	3.8
Cellular uptake (nmol Ru/mg of cell protein)	2.11 ± 0.12	2.12 ± 0.33	0.78 ± 0.03	0.90 ± 0.03	2.05 ± 1.35

Finally, the EC_{50} values for the cyclometalated compound [**4**]PF_6 were found to be 0.086 and 0.18 µM in the dark for A549 and PC3pro4 cells respectively, and 0.075 and 0.070 µM after green light irradiation, leading to negligible PI's of 1.1 and 2.6 for A549 and PC3pro4 cells, respectively. A comparable intracellular concentration (0.90 nmol Ru per mg of cell proteins) to that of [**3**]Cl_2 was obtained when treating with a 2000-fold lower dose of the cyclometalated complex [**4**]PF_6 (0.08 µM), which highlights the dramatic effect of the lower charge (+1) of this complex on the lipophilicity and passive uptake of the complex, compared to the rest of the series. In general, this series of ruthenium complexes showed a lower cytotoxicity in the dark

against PC3pro4 cells than against A549 cells, whereas the light-activated EC_{50} values were in the same range for both cell lines. This results in a greater PI in PC3pro4 cells compared to A549 cells.

Table 6.3. Cytotoxicity expressed as effective concentrations (EC_{50} with 95% confidence intervals, in µM) of [1]Cl$_2$, [2](PF$_6$)$_2$, [3]Cl$_2$, [4]PF$_6$, [5]Cl$_2$, and Rose Bengal in lung (A549) and prostate (PC3pro4) cancer cell lines, under normoxia and hypoxia, in the dark and upon green light irradiation (520 nm).

Cell line	Light dose (J.cm^{-2})	[1]Cl$_2$	[2](PF$_6$)$_2$	[3]Cl$_2$	[4]PF$_6$	[5]Cl$_2$	Rose Bengal
A549 21% O$_2$	0	3.4 (+0.97/−0.76)	59 (+17/−13)	>500 (−/−)	0.086 (+0.029/−0.022)	3.4 (+0.39/−0.35)	>50 (−/−)
	18.8	0.62 (+0.14/−0.11)	6.5 (+2.4/−1.8)	71 (+25/−18)	0.075 (+0.027/−0.022)	0.26 (+0.11/−0.08)	1.2 (+0.39/−0.30)
	PI	5.5	9.1	>7	1.1	13	>40
PC3pro4 21% O$_2$	0	4.7 (+0.32/−0.30)	142 (+83/−52)	>500 (−/−)	0.18 (+0.028/−0.024)	5.1 (+1.6/−1.2)	29 (+2.3/−2.1)
	18.8	0.79 (+0.028/−0.027)	3.2 (+0.65/−0.54)	33 (+2.9/−2.6)	0.070 (+0.016/−0.013)	0.22 (+0.025/−0.022)	0.067 (+0.60/−0.066)
	PI	6.0	45	>15	2.6	23	>400
PC3pro4 1% O$_2$	0	8.1 (1.4/−1.2)	>100 (−/−)	>500 (−/−)	0.51 (+0.27/−0.18)	14 (+1.3/−1.2)	25 (+2.9/−2.6)
	18.8	5.4 (+0.79/−0.69)	78 (+28/−21)	312 (+121/−87)	0.66 (+0.41/−0.25)	8.4 (+2.0/−1.6)	9.9 (+3.0/−2.3)
	PI	1.5	>1.3	>1.6	-	1.7	2.5

To investigate the possible relation between $^1O_2$ generation and the observed cytotoxicity, the cytotoxicity of the six compounds was tested under hypoxic conditions, in which $^1O_2$ generation is seriously impaired. As shown in Figure AVII.3, cell cultures of both A549 and PC3pro4 were viable under hypoxia, showing slower growth curves compared to normoxia. Considering the higher PI observed for PC3pro4 than for A549, only PC3pro4 cells were used in the cytotoxicity assays under hypoxia. The protocol was similar to the one used for normoxia, except that dioxygen concentrations were kept at 1% during cell culturing and light irradiation, as described recently by Lameijer *et al.*[13] Under such conditions, Rose Bengal showed similar cytotoxicity in the dark but a much lower cytotoxicity after green light irradiation (EC_{50} = 9.9 µM, Table 6.3) compared to normoxia, resulting in a PI of only 2.5. The

ruthenium-based photosensitizer [**5**]Cl$_2$ also showed a decreased PI of 1.7, as well as a general increase of the EC$_{50}$ values both in the dark and after light irradiation. Overall, working at 1% O$_2$ decreased substantially the photo index of PDT photosensitizers, as reported previously.[7] For compounds [**1**]Cl$_2$, [**2**](PF$_6$)$_2$, and [**3**]Cl$_2$ EC$_{50}$ values of 8.1, >100, and >500 µM were found in the dark, and of 5.4, 78, and 312 µM after green light irradiation, corresponding to PI's of 1.5, >1.3, and >1.6, respectively. Although after light activation EC$_{50}$ values were still rather high, the cell viability curves (Figure 6.4) showed a clearly enhanced cytotoxicity upon light irradiation. The extremely low cytotoxicity of [**2**](PF$_6$)$_2$ and [**3**]Cl$_2$ in the dark (>100 and >500 µM, respectively), did not allow for an accurate calculation of the PI.
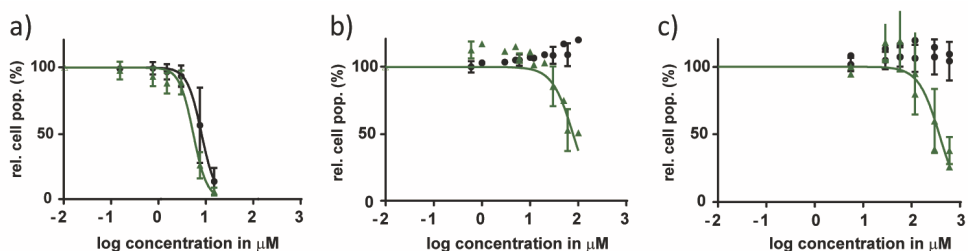

*Figure 6.4. Dose-response curves for PC3pro4 cells under hypoxia treated with [**1**]Cl$_2$, [**2**](PF$_6$)$_2$, or [**3**]Cl$_2$ and irradiated with green light (520 nm, 18.8 J·cm^{-2}) 24 h after treatment (green data points) or left in the dark (black data points).*

6.3 Discussion

A first analysis of the data suggests a cell dependency of the cytotoxicity of all the complexes in the series. Indeed, higher PI's were found for PC3pro4 cells than for A549 cells under normoxia. However, a more careful analysis of the data is necessary by calculating the p-value, *i.e.* the statistical significance of the differences in EC$_{50}$ values. When comparing the cytotoxicity of complexes [**1**]Cl$_2$, [**2**](PF$_6$)$_2$, and [**3**]Cl$_2$ against PC3pro4 and A549 cell p-values ranging from 0.0328 to 0.585 were obtained, both in the dark and after light irradiation. These values are at or beyond the limit of statistical significance ($p < 0.05$). Thus, a cell-selectivity of the series of complexes towards PC3pro4 under normoxia cannot be stated.

On the other hand, a lower cytotoxicity was observed under hypoxia, which is usually attributed to the acquired chemoresistance of cancer cells under such conditions.[8] Indeed, PC3pro4 cells were passaged twice under hypoxia before performing the phototoxicity assay, which selected *in situ* the most resistant cells capable of surviving under harsher conditions. Nevertheless, another factor has to be considered *in vitro*:

varying the concentration of O_2 modifies cell confluence. As shown in the growth curves (Appendix VII and Figure AVII.5), at the time of treatment and irradiation of the cells (<48 h after seeding) the cell confluence of PC3pro4 cells under normoxia and hypoxia were similar. However, during the following 48 h the cell growth under normoxia was much faster than that under hypoxia, resulting in a much lower cell density in the latter. This difference in cell density might have a great impact on the observed cytotoxicity.[26]

As suggested by Lameijer *et al*., validating a compound as either a PACT or a PDT agent requires comparing the PI's, not the EC_{50} values.[13] On the one hand, the PI of 2.6 observed under normoxia for [**4**]PF_6 in PC3pro4 cells seems encouraging, while the extraordinary high cytotoxicity found in the dark agrees with previous reports on cyclometalated complexes.[27] However, the negligible PI observed under hypoxia is strongly indicative of a photodynamic effect under normoxia, which is confirmed by the relatively high Φ_Δ value (0.19) found for this complex. In other words, although photosubstitution is possible with [**4**]$^+$ its phototoxicity seem here to be a consequence of ROS and most probably singlet oxygen generation. A similar observation was made for [**1**]Cl_2, the PI of which dropped from 6.0 to 1.5 when decreasing the O_2 concentration from 21% to 1%. For that complex, however, the very low Φ_Δ value (0.020) cannot explain the light-induced cell death. Here we suggest a PDT type I, or a dual PDT-PACT mode of action, to explain the PI observed under normoxia. Finally, for complexes [**2**]$(PF_6)_2$ and [**3**]Cl_2 accurate PI values could not be determined due to the extremely low cytotoxicity found in the dark under hypoxia. However, the cytotoxicity is clearly enhanced after light irradiation (Figure 6.4). Even if the EC_{50} values remain rather high after light irradiation one should not discard these two compounds, but instead the biological relevance of our 2D cell monolayer protocol should first be evaluated by using alternative models of hypoxic cancer, such as 3D tumor spheroids.

6.4 Conclusions

In conclusion, we have shown the dependency of the cell uptake and (photo)cytotoxicity on the lipophilicity in a series of ruthenium(II) complexes bearing a non-toxic photolabile ligand. Furthermore, we have shown that the cytotoxicity of all the compounds is lower under hypoxia compared to that under normoxia probably due to the acquired chemoresistance of hypoxic cells. However, upon green light irradiation, the cytotoxicity of the PACT complex [**2**]$(PF_6)_2$ was clearly enhanced, which is the first experimental demonstration of light-induced cytotoxicity under

hypoxia for a metal-based PACT compound releasing a non-toxic organic ligand. Since PDT type II would be unlikely due to both the low oxygen concentration and the low Φ_Δ of PACT compounds, we are close here to prove that the cytotoxicity of PACT complexes based on N,S photolabile ligands is indeed oxygen-independent. However, more work on cell death mechanism and the mode of action of these compounds should be performed, if possible in hypoxic 3D tumor spheroids, to conclude on the medicinal potential of this series of compounds.

6.5 Experimental

6.5.1 Synthesis

General: The ligands 2,2'-bipyridine (bpy), 6,6'-dimethyl-2,2'-bipyridine (dmbpy), and 4,7-diphenyl-1,10-phenanthroline (Ph$_2$phen) were purchased from Sigma-Aldrich. Potassium hexafluoridophosphate (KPF$_6$) was purchased from Alfa-Aesar. All reactants and solvents were used without further purification. The synthesis of *cis*-[Ru(dmbpy)$_2$Cl$_2$], [Ru(Ph$_2$phen)$_2$(bpy)]Cl$_2$ ([**5**]Cl$_2$), and 2-(methylthio)methylypridine (mtmp) was carried out according to literature procedures.[14, 28-29] The synthesis of [**1**]Cl$_2$ and [**4**]PF$_6$ is described in Chapter 3 and Chapter 5, respectively. Electrospray mass spectra (ES MS) were recorded by using a MSQ Plus Spectrometer. All ^{1}H NMR spectra were recorded on a Bruker DPX-300 or DMX-400 spectrometers. Chemical shifts are indicated in ppm relative to the residual solvent peak.

[Ru(Ph$_2$phen)(DMSO)$_2$Cl$_2$] [**7**]: *cis*-[Ru(DMSO)$_4$Cl$_2$] (500 mg, 1.0 mmol) and 4,7-diphenyl-1,10-phenanthroline (340 mg, 1.0 mmol) were heated at reflux in ethanol (35 mL) for 2 h. The reaction was then cooled to room temperature and the solvent volume reduced to *ca.* 10 mL *in vacuo*. The precipitate that formed upon cooling was filtered, washed with minimal cold ethanol and copious amounts of hexane/diethyl ether, and dried under vacuum. Yield: light-brown solid, 350 mg (0.52 mmol, 51%). ^{1}H NMR (400 MHz, CDCl$_3$) δ 10.19 (dd, J = 5.5, 0.9 Hz, 1H), 10.00 (dd, J = 5.6, 0.9 Hz, 1H), 8.07 – 7.99 (m, 2H), 7.89 (dd, J = 5.5, 0.9 Hz, 1H), 7.72 (dd, J = 5.6, 0.9 Hz, 1H), 7.63 – 7.51 (m, 10H), 3.67 (s, 3H), 3.62 (s, 3H), 3.27 (s, 3H), 2.70 (s, 3H). ^{13}C NMR (101 MHz, CDCl$_3$) δ 155.72, 152.34, 149.95, 148.98, 135.93, 135.79, 129.81, 129.68, 129.13, 128.73, 128.27, 125.49, 125.36, 125.30, 125.23, 47.15, 46.52, 45.49, 44.37.

[Ru(Ph$_2$phen)(ox)(mtmp)] [**8**]: [**7**] (300 mg, 0.45 mmol) and sodium oxalate (85 mg, 0.65 mmol) were heated at reflux in water (15 mL) for 1 h. The reaction was then cooled to room temperature and added to a hot (~60 °C) solution of 2-

(methylthio)methylpyridine (63 mg, 0.45 mmol) in ethylene glycol (15 mL). The resulting mixture was heated at reflux for 3 h, cooled to room temperature, and added dropwise to 50 mL of stirring water. After 30 min, the precipitate was filtered through a 1 μm membrane. The solids were washed with copious amounts of water and minimal acetone before drying thoroughly under vacuum. The mixture of isomers was separated by silica column ($R_f = 0.3$) in CH_2Cl_2/CH_3OH (2 − 20% CH_3OH). Only one isomer was isolated. Yield: dark red powder, 140 mg (0.21 mmol, 71%). ^{1}H NMR (400 MHz, CDCl$_3$) δ 9.63 (dd, J = 5.6, 0.9 Hz, 1H), 9.34 (dd, J = 5.4, 0.9 Hz, 1H), 8.08 (qd, J = 9.4, 0.9 Hz, 2H), 7.81 (d, J = 5.3 Hz, 1H), 7.66 − 7.46 (m, 11H), 7.44 − 7.35 (m, 2H), 6.84 − 6.78 (m, 1H), 6.59 (td, J = 6.1, 2.4 Hz, 1H), 4.70 (d, J = 13.4 Hz, 1H), 4.61 (d, J = 13.5 Hz, 1H), 2.45 (s, 3H). ^{13}C NMR (101 MHz, CDCl$_3$) δ 168.86, 167.83, 163.08, 153.42, 152.04, 151.05, 149.48, 148.15, 145.53, 136.37, 136.29, 134.29, 129.96, 129.78, 129.53, 129.35, 129.21, 129.17, 129.03, 128.39, 125.91, 125.48, 124.44, 123.14, 122.34, 45.79, 16.12. Anal. Calcd for $C_{33}H_{25}N_3O_4RuS\cdot3H_2O$: C, 55.45; H, 4.37; N, 5.88 Found: C, 56.08; H, 4.56; N, 5.46.

[Ru(bpy)(Ph₂phen)(mtmp)](PF₆)₂ [2](PF₆)₂: **[8]** (140 mg, 0.21 mmol) was suspended in CH_3CN (3 mL) and then perchloric acid 1 M (3 mL) was added. After refluxing for 1 h, a red-brown solution containing the ruthenium-solvate was obtained and, after cooling, it was poured in stirring water (15 mL). The orange solid that precipitated was filtered and dried to yield [Ru(Ph₂phen)(mtmp)(CH₃CN)₂](ClO₄)₂. The intermediate was dissolved in an ethylene glycol solution (15 mL) containing the bpy ligand (33 mg, 0.21 mmol) and heated at 100 °C for 6 h. The deep red mixture was cooled to room temperature and poured in stirring aqueous KPF₆ solution to precipitate the crude complex as the hexafluoridophosphate salt. Configurational isomers were resolved by column chromatography on silica CH_2Cl_2/CH_3OH 95:5. Three fractions were obtained from a long orange band ($R_f \sim 0.5$), from which only the last fraction contained a pure isomer (3.2 mg, 2%, Isomer B, **[2b]**(PF₆)₂). A mixture of isomers A/B in a ration 0.23:1 has been used (60 mg, 28%). ^{1}H NMR (400 MHz, CD₃CN) δ 9.63 (d, J = 5.5 Hz, 1H$_B$), 9.39 (d, J = 5.7 Hz, 1H$_A$), 8.61 (d, J = 8.2 Hz, 1H$_B$), 8.58 − 8.51 (m, 2H$_A$), 8.43 (d, J = 8.1 Hz, 1H$_B$), 8.31 (dd, J = 8.0, 1.5 Hz, 1H$_B$), 8.29 − 8.23 (m, 1H$_B$ + 1H$_A$), 8.22 − 8.14 (m, 2H$_B$ + 2H$_A$), 8.14 − 8.03 (m, 3H$_A$), 8.02 (d, J = 5.5 Hz, 1H$_B$), 7.99 (d, J = 5.5 Hz, 1H$_B$), 7.93 (ddd, J = 7.8, 6.5, 1.5 Hz, 1H$_B$), 7.86 (td, J = 7.8, 1.6 Hz, 1H$_A$), 7.81 − 7.51 (m, 15H$_B$ + 15H$_A$), 7.48 (dd, J = 5.9, 1.5 Hz, 1H$_A$), 7.32 (ddd, J = 7.1, 5.6, 1.3 Hz, 1H$_A$), 7.24 (d, J = 5.5 Hz, 1H$_B$), 7.17 (td, J = 7.2, 5.6, 1.4 Hz, 1H$_B$ + 1H$_A$), 6.98 (ddd, J = 7.7, 5.8, 1.6 Hz, 1H$_B$), 4.82 (d, J = 16.5 Hz, 1H$_B$), 4.74 (d, J = 16.7 Hz, 1H$_A$), 4.28 (dd, J = 16.6, 4.8 Hz, 1H$_B$ + 1H$_A$), 1.59 (s, 3H$_B$), 1.32 (s, 3H$_A$). ^{13}C NMR (101

MHz, CD$_3$CN) δ 162.96, 162.63, 158.56, 157.73, 153.51, 153.33, 153.09, 152.90, 151.98, 150.77, 150.61, 150.05, 149.66, 148.72, 139.46, 138.67, 138.55, 136.62, 136.53, 130.79, 130.70, 130.13, 130.06, 129.20, 127.78, 127.26, 127.19, 127.12, 126.92, 125.86, 125.59, 125.55, 124.93, 45.36, 17.04. High Resolution ES MS m/z (calcd): 364.57519 (364.57446, [**2**]$^{2+}$), 874.11407 (874.11365, [**2** + PF$_6$]$^+$). Anal. Calcd for C$_{41}$H$_{33}$F$_{12}$N$_5$P$_2$RuS: C, 48.34; H, 3.26; N, 6.87 Found: C, 48.21; H, 3.41; N, 6.82.

[Ru(dmbpy)$_2$(mtmp)]Cl$_2$ [3]Cl$_2$: [Ru(dmbpy)$_2$Cl$_2$] (750 mg, 1.4 mmol), Et$_3$N (200 μL, 1.4 mmol), and mtmp (190 mg, 1.4 mmol) were dissolved in deaereted ethylene glycol (10 mL) and heated under N$_2$ at 100 °C for 15 min. After the reaction mixture was cooled to room temperature, water (20 mL) was added and the mixture was washed with CH$_2$Cl$_2$ (3 × 20 mL). A saturated aqueous KPF$_6$ solution was added to the water layer and the complex was extracted with CH$_2$Cl$_2$ (3 × 20 mL). After reducing the volume of CH$_2$Cl$_2$ (5 mL), a saturated acetone Bu$_4$NCl solution (15 mL) was added to the CH$_2$Cl$_2$ mixture and put in an ice bath for 15 min. A red precipitate was afforded, which was filtered and washed with acetone and diethyl ether. Yield: 750 mg (60%). ^{1}H NMR (300 MHz, D$_2$O) δ 8.35 – 8.26 (m, 2H), 8.24 (d, J = 8.1 Hz, 1H), 8.07 (t, J = 7.9 Hz, 1H), 8.03 – 7.96 (m, 2H), 7.93 (t, J = 7.9 Hz, 1H), 7.74 – 7.61 (m, 2H), 7.55 (d, J = 7.7 Hz, 1H), 7.45 (t, J = 7.9 Hz, 2H), 7.39 – 7.32 (m, 2H), 7.28 (d, J = 7.8 Hz, 1H), 7.10 (t, J = 6.7 Hz, 1H), 4.11 (d, J = 17.8 Hz, 1H), 3.96 (d, J = 17.8 Hz, 1H), 2.77 (s, 3H), 2.23 (s, 3H), 2.04 (s, 3H), 1.76 (s, 3H), 0.97 (s, 3H). ^{13}C NMR (75 MHz, D$_2$O) δ 167.00, 166.55, 166.28, 166.14, 162.14, 159.57, 159.41, 159.37, 159.19, 154.98, 138.44, 138.37, 137.84, 137.54, 137.48, 127.62, 127.24, 127.16, 125.83, 123.89, 123.53, 122.31, 122.10, 121.13, 120.76, 44.93, 26.63, 24.95, 23.79, 23.46, 16.15. High Resolution ES MS m/z (calcd): 304.57488 (304.57446, [**3**]$^{2+}$).

6.5.2 Single Crystal X-Ray crystallography

General: All reflection intensities were measured at 110(2) K using a SuperNova diffractometer (equipped with Atlas detector) with Mo $K\alpha$ radiation (λ = 0.71073 Å) under the program CrysAlisPro (Version CrysAlisPro 1.171.39.29c, Rigaku OD, 2017). The same program was used to refine the cell dimensions and for data reduction. The structure was solved with the program SHELXS-2014/7 and was refined on F^2 with SHELXL-2014/7.[30] Numerical absorption correction based on gaussian integration over a multifaceted crystal model was applied using CrysAlisPro. The temperature of the data collection was controlled using the system Cryojet (manufactured by Oxford Instruments). The H atoms were placed at calculated positions (unless otherwise specified) using the instructions AFIX 23, AFIX 43, AFIX

137 or AFIX 147 with isotropic displacement parameters having values 1.2 or 1.5 Ueq of the attached C or O atoms. The H atoms attached to O1W (lattice water molecule) were found from difference Fourier maps, and their coordinates were refined freely.

Crystal growing: [**3**]Cl$_2$ (1.0 mg) was dissolved in methanol (1 mL, 1.5 mM) and transfered (650 µL) into a GC vial, which was placed in a larger vial that contained diisopropyl ether (2700 µL) as a counter solvent. The large vial was stoppered. After a few days quality crystals suitable for X-ray structure determination were obtained by vapor diffusion.

Details of the crystal structure: The structure is ordered except for a small amount of very disordered (probably partially occupied or even a mixture of) lattice molecules in the crystal lattice. Their contribution has been removed from the final refinement using the SQUEEZE procedure in Platon.[31] $0.54 \times 0.41 \times 0.11$ mm^3, triclinic, *P-1*, a = 10.4877(3), b = 12.1635(3), c = 14.3238(3) Å, α = 104.346(2), β = 98.3169(19), γ = 99.403(2)°, V = 1713.41(8) Å^3, Z = 2, μ = 0.71 mm^{-1}, T_{min}–T_{max}: 0.250-1.000. 27712 reflections were measured up to a resolution of $(\sin \theta/\lambda)_{max}$ = 0.650 Å^{-1}. 7878 reflections were unique (R_{int} = 0.023), of which 7423 were observed [$I > 2\sigma(I)$]. 401 parameters were refined using 3 restraints. $R1/wR2$ [$I > 2\sigma(I)$]: 0.02180/0.0515. $R1/wR2$ [*all reflections*]: 0.0238/0.0527. S = 1.046. Residual electron density found between −0.65 and 0.52 e Å^{-3}.

6.5.3 Photochemistry

When monitoring photoreactions with UV-vis spectroscopy and mass spectrometry, a Cary 50 Varian spectrometer equipped with temperature control set to 298 K and a LED light source (λ_{ex} = 521 nm, with a Full Width at Half Maximum of 33 nm) with a photon flux between 2.39 and $6.25 \cdot 10^{-8}$ mol·s^{-1} was used. The irradiation experiments were performed in a quartz cuvette containing 3 mL of solution. A stock solution of the desired complex was prepared using either H$_2$O or CH$_3$CN, which was then diluted in the cuvette to a working solution concentration. The sample was deaerated 15 min by gentle bubbling of N$_2$ and the atmosphere was kept inert during the experiment by a gentle flow of N$_2$ on top of the cuvette. A UV-vis spectrum was measured every 30 s for the first 10 min, every 1 min for the next 10 min, and eventually every 10 min until the end of the experiment. Data was analysed with Microsoft Excel. Experimental conditions are detailed in Table 6.4.

Table 6.4. Conditions of the photoreactions monitored with MS and UV-vis.

Complex	Solvent	Stock solution			Working sol. (mM)	Photon flux (mol·s^{-1})
		w (mg)	V (mL)	M (mM)		
[**2**](PF$_6$)$_2$	CH$_3$CN	1.1	10	0.108	0.036	6.21·10^{-8}
[**3**]Cl$_2$	CH$_3$CN	0.9	10	0.132	0.088	6.25·10^{-8}
[**3**]Cl$_2$	H$_2$O	1.0	10	0.147	0.073	2.39·10^{-8}

6.5.4 Cell culture and EC$_{50}$ (photo)cytotoxicity assay

The PC3pro4 cell line was provided by Prof. Dr. Ewa Snaar-Jagalska. Following the protocol described in Appendix II, 24 h after seeding A549 (5,000 and 6,000 cells/well under normoxic and hypoxic conditions, respectively) or PC3pro4 cells (4,000 cells/well under both normoxic and hypoxic conditions), aliquots (100 µL) of six different concentrations of freshly prepared stock solutions of [**1**]Cl$_2$, [**2**](PF$_6$)$_2$, [**3**]Cl$_2$, [**4**]PF$_6$, [**5**]Cl$_2$, or Rose Bengal in OptiMEM were added. Plates were incubated in the dark for an additional 24 h. After this period, half of the plates were irradiated with green light (λ_e = 520 nm, light dose = 18.8 J·cm^{-2}) and the other half were kept in the dark. After irradiation, all the plates were incubated for an additional 48 h before fixation and cell quantification using an SRB assay. As shown in Figure AVII.2, after 15 min irradiation (18.8 J·cm^{-2} using the normoxic setup) all the complexes seem fully photoactivated, except for complex [**4**]PF$_6$ and [**5**]Cl$_2$. The first has indeed a very low photosubstitution quantum yield (Chapter 5) and it should be irradiated for too long to achieve full activation. The latter, like its analogue [Ru(bpy)$_3$]Cl$_2$, does not photosubstitute any of the ligands but deactivates by phosphorescence emission.

The protocol followed under hypoxic conditions has been described previously by Lameijer *et al.*[13] In short, cells were passaged at least twice under hypoxia (1% O$_2$), before performing the (photo)cytotoxicity assay. The light irradiation was performed using a small incubator with a glass cover in order to irradiate while keeping the atmosphere at 1% O$_2$. Due to the glass cover the power intensity of the LED array is lower than that in the irradiation set up for normoxic conditions.[13] Thus, 27.5 min of green light irradiation in the hypoxic setup corresponded to the same light dose as 15 min irradiation in the normoxic setup (18.8 J·cm^{-2}).

6.5.5 Cellular uptake

Cell uptake studies for complexes [**1**]Cl$_2$, [**2**](PF$_6$)$_2$, [**3**]Cl$_2$, [**4**]PF$_6$, and [**5**]Cl$_2$ were conducted on A549 lung cancer cells. 1.6·10^6 cells were seeded in OptiMEM complete

(10 mL) in 75 cm^2 T-flasks at t = 0 h. At t = 24 h the media was aspirated and cells were treated with solutions of [**1**]Cl$_2$, [**2**](PF$_6$)$_2$, [**3**]Cl$_2$, [**4**]PF$_6$, or [**5**]Cl$_2$ to give a final concentration at the EC$_{50}$ in the dark (3.4, 65, 160, 0.08, and 3.8 μM, respectively) in a total volume of 10 mL. After 24 h of drug incubation at 37 ºC and 21% O$_2$, the medium was aspirated and the cells were washed twice with PBS (5 mL). Then, the cells were trypsinized (2 mL), suspended with OptiMEM (8 mL), and centrifuged (1200 rpm, 4 min). After aspiration of the supernatant, the cells were resuspended in PBS (1 mL) and counted. After a second centrifugation, the supernatant was discarded. For metal and protein quantification, the pellets were resuspended in demineralized water (250 μL) and lysed for 30 min by ultrasonication. The protein content of lysates was determined by the Bradford method, and the ruthenium content was determined by Atomic Absorption Spectroscopy.

A contrAA 700 high-resolution continuum-source atomic absorption spectrometer (Analytik Jena AG) was used. Pure samples of the respective complex was used as standard and calibration was done in a matrix-matched manner (meaning all samples and standards were adjusted to the same cellular protein concentration of 1.0 mg/mL by dilution with distilled water if necessary). Triton-X 100 (1%, 10 μL), as well as nitric acid (13%, 10 μL), were added to each standard sample (100 μL). Samples were injected (25 μL) into coated standard graphite tubes (Analytik Jena AG) and thermally processed as previously described by Schatzschneider *et al.*[32] Drying steps were adjusted and the atomization temperature set to 2400 °C. Ruthenium was quantified at a wavelength of 349.90 nm. The mean integrated absorbance of double injections were used throughout the measurements. The data from two independent biological replications was used to obtain the uptake values shown in Table 6.2.

6.6 References

1. T. Sainuddin, M. Pinto, H. Yin, M. Hetu, J. Colpitts and S. A. McFarland, *J. Inorg. Biochem.*, **2016**, 158, 45-54.
2. K. T. Hufziger, F. S. Thowfeik, D. J. Charboneau, I. Nieto, W. G. Dougherty, W. S. Kassel, T. J. Dudley, E. J. Merino, E. T. Papish and J. J. Paul, *J. Inorg. Biochem.*, **2014**, 130, 103-111.
3. B. S. Howerton, D. K. Heidary and E. C. Glazer, *J. Am. Chem. Soc.*, **2012**, 134, 8324-8327.
4. J. A. Cuello-Garibo, M. S. Meijer and S. Bonnet, *Chem. Commun.*, **2017**, 53, 6768-6771.
5. Q.-X. Zhou, W.-H. Lei, J.-R. Chen, C. Li, Y.-J. Hou, X.-S. Wang and B.-W. Zhang, *Chem. - Eur. J.*, **2010**, 16, 3157-3165.
6. H. Huang, B. Yu, P. Zhang, J. Huang, Y. Chen, G. Gasser, L. Ji and H. Chao, *Angew. Chem.*, **2015**, 127, 14255-14258.
7. J. Fong, K. Kasimova, Y. Arenas, P. Kaspler, S. Lazic, A. Mandel and L. Lilge, *Photochem. Photobiol. Sci.*, **2015**, 14, 2014-2023.
8. W. R. Wilson and M. P. Hay, *Nat. Rev. Cancer*, **2011**, 11, 393-410.
9. N. M. Mazure, *Nature*, **2006**, 441, 437.

10. B. Keith and M. C. Simon, *Cell*, **2007**, 129, 465-472.
11. A. M. Weljie and F. R. Jirik, *Int. J. Biochem. Cell Biol.*, **2011**, 43, 981-989.
12. S. Rockwell, I. T. Dobrucki, E. Y. Kim, S. T. Marrison and V. T. Vu, *Curr. Mol. Med.*, **2009**, 9, 442-458.
13. L. N. Lameijer, D. Ernst, S. L. Hopkins, M. S. Meijer, S. H. C. Askes, S. E. Le Dévédec and S. Bonnet, *Angew. Chem., Int. Ed.*, **2017**, 56, 11549-11553.
14. O. Mazuryk, K. Magiera, B. Rys, F. Suzenet, C. Kieda and M. Brindell, *JBIC, J. Biol. Inorg. Chem.*, **2014**, 19, 1305-1316.
15. C. S. Burke and T. E. Keyes, *Rsc Advances*, **2016**, 6, 40869-40877.
16. J. H. Wallenstein, J. Sundberg, C. J. McKenzie and M. Abrahamsson, *Eur. J. Inorg. Chem.*, **2016**, 897-906.
17. C. Mari, V. Pierroz, R. Rubbiani, M. Patra, J. Hess, B. Spingler, L. Oehninger, J. Schur, I. Ott, L. Salassa, S. Ferrari and G. Gasser, *Chem. - Eur. J.*, **2014**, 20, 14421-14436.
18. A. Frei, R. Rubbiani, S. Tubafard, O. Blacque, P. Anstaett, A. Felgentrager, T. Maisch, L. Spiccia and G. Gasser, *J. Med. Chem.*, **2014**, 57, 7280-7292.
19. G. Shi, S. Monro, R. Hennigar, J. Colpitts, J. Fong, K. Kasimova, H. Yin, R. DeCoste, C. Spencer, L. Chamberlain, A. Mandel, L. Lilge and S. A. McFarland, *Coord. Chem. Rev.*, **2015**, 282–283, 127-138.
20. D. Garcìa-Fresnadillo, Y. Georgiadou, G. Orellana, A. M. Braun and E. Oliveros, *Helv. Chim. Acta*, **1996**, 79, 1222-1238.
21. C. Tanielian and C. Wolff, *J. Phys. Chem.*, **1995**, 99, 9825-9830.
22. S. L. Hopkins, B. Siewert, S. H. C. Askes, P. Veldhuizen, R. Zwier, M. Heger and S. Bonnet, *Photochem. Photobiol. Sci.*, **2016**, 15, 644-653.
23. C. A. Pettaway, S. Pathak, G. Greene, E. Ramirez, M. R. Wilson, J. J. Killion and I. J. Fidler, *Clin. Cancer Res.*, **1996**, 2, 1627-1636.
24. R. W. Horobin, J. C. Stockert and F. Rashid-Doubell, *Histochem. Cell Biol.*, **2006**, 126, 165-175.
25. C. A. Puckett and J. K. Barton, *J. Am. Chem. Soc.*, **2007**, 129, 46-47.
26. T. L. Riss and R. A. Moravec, *Assay Drug Dev. Technol.*, **2004**, 2, 51-62.
27. L. Fetzer, B. Boff, M. Ali, M. Xiangjun, J.-P. Collin, C. Sirlin, C. Gaiddon and M. Pfeffer, *Dalton Trans.*, **2011**, 40, 8869-8878.
28. J. P. Collin and J. P. Sauvage, *Inorg. Chem.*, **1986**, 25, 135-141.
29. E. Reisner, T. C. Abikoff and S. J. Lippard, *Inorg. Chem.*, **2007**, 46, 10229-10240.
30. G. M. Sheldrick, *Acta Crystallogr., Sect. A: Found. Adv.*, **2008**, 64, 112-122.
31. A. L. Spek, *Acta Crystallogr., Sect. D: Biol. Crystallogr.*, **2009**, 65, 148-155.
32. U. Schatzschneider, J. Niesel, I. Ott, R. Gust, H. Alborzinia and S. Wölfl, *ChemMedChem*, **2008**, 3, 1104-1109.